Mechanics of Materials 140 (2020) 103243

Contents lists available at ScienceDirect

Mechanics of Materials

journal homepage: www.elsevier.com/locate/mechmat

Bioinspired toughness improvement through soft interlayers in mineral reinforced polypropylene

Johannes Wiener[a], Florian Arbeiter[a,*], Abhishek Tiwari[b,c], Otmar Kolednik[b], Gerald Pinter[a]

[a] Materials Science and Testing of Polymers, Montanuniversitaet Leoben, 8700 Leoben, Austria
[b] Erich-Schmid-Institute of Materials Science, Austrian Academy of Science, 8700 Leoben, Austria
[c] Materials Center Leoben GmbH, 8700 Leoben, Austria

ARTICLE INFO

Keywords:
Polypropylene
Multi-layer
Fracture toughness
Material inhomogeneity
J-integral

ABSTRACT

The effects of soft, polymeric interlayers on a brittle, mineral reinforced polymer matrix are investigated. Interlayers made of a standard polypropylene (PP) and a soft type of PP are introduced into matrix materials of either highly or moderately mineral particle reinforced PP. Single edge notch bending experiments are performed to characterize the fracture toughness of these composites. The experimental *J*-integral J_{exp} is used to describe the fracture toughness of the investigated materials. The multi-layered materials are compared to the homogeneous matrix material. A modified plotting technique is applied to more distinctly demonstrate the effects of soft layers on J_{exp} as a function of the crack extension Δa. The fracture toughness is evaluated and the slope of the J-Δa curves is used as a qualitative measure of crack growth resistance. In addition, the crack growth rate is recorded. The results show improvements in fracture toughness of almost twenty times of the matrix material, provided the material combination is chosen properly. This increase in fracture toughness is achieved due to a crack-arresting effect in the soft layers, which is followed by an energy-expensive crack re-initiation step.

1. Introduction

A multitude of technical applications strive for a high stiffness and/or high strength to support large loads. Furthermore, a high toughness can be equally important in order to prevent catastrophic failure of vital structures. Unfortunately, these characteristics are often mutually exclusive in engineering materials (Ashby and Cebon 1993; Ritchie 2011). Usually the most reasonable compromise between stiffness and toughness has to be selected as the material of choice. However, for biological materials, the same restrictions do not seem to apply (Jia et al., 2019). The majority of biological materials with load bearing functionality exhibit an astonishingly high fracture toughness, especially when considering their seemingly brittle composition. Close examination of biomaterials reveals that they do not show a homogeneous microstructure but rather complex and elegant hierarchical structures. Additionally, many of these structures also feature secondary functionalities besides the load bearing component. For example, bone tissue is not only designed to support weight and movement related forces of the body. It serves as reservoir for nutrients and minerals while also producing vital components of blood (Morgan et al., 2013).

Two examples of structured bio-materials with a high content of brittle matrix are nacre, which mainly consists of aragonite ($CaCO_3$) with a negligible amount of protein (Barthelat and Espinosa 2007; Song et al., 2018), as well as the skeleton of the deep sea sponge *Euplectella aspergillum* which also consists of over 99% SiO_2 (bio-glass) and only a small amount of organic material (Aizenberg et al., 2005; Miserez et al., 2008; Woesz et al., 2006; Levi et al., 1989; Müller et al., 2008).

Much research has been conducted on the subject of nacre. On a microscopic scale, the material consists of many interlocking hexagonal platelets (Figs. 1a and b). While the platelets themselves are made of aragonite, the small layers in between them consist of soft and elastic protein. The increase in toughness compared to pure aragonite can be attributed to several different mechanisms. These include platelet pullout, platelet interlocking and the obvious increase in fracture surface (Barthelat and Espinosa 2007; Zhao et al., 2018; Dutta et al., 2013). Recent studies also showed great results for parts produced by 3D-inkjet printing of polymeric resins (Jia et al., 2019; Jia and Wang 2019; Yadav et al., 2018). In all of these applications, the intricate microstructure and their complex deformation and fracture behaviors (Barthelat and Espinosa 2007; Song et al., 2018; Miserez et al., 2008; Dutta et al., 2013; Dutta and Tekalur 2014) lead to improved fracture

* Corresponding author.
E-mail address: Florian.Arbeiter@unileoben.ac.at (F. Arbeiter).

https://doi.org/10.1016/j.mechmat.2019.103243
Received 24 July 2019; Received in revised form 7 November 2019; Accepted 7 November 2019
Available online 09 November 2019

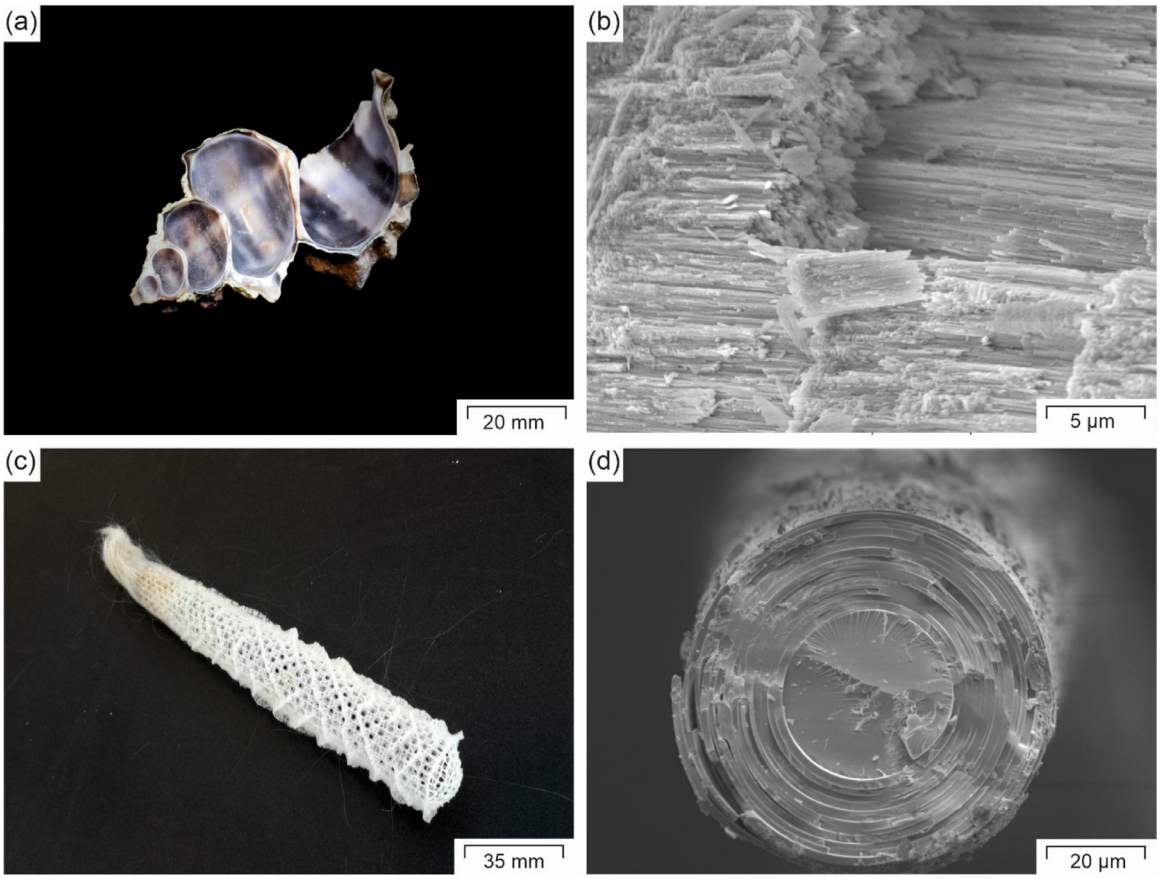

Fig. 1. Structure of biological materials: Conch Shell (a) and its platelet-like microstructure (b) and the deep-sea sponge (c) with its concentric microstructure (d).

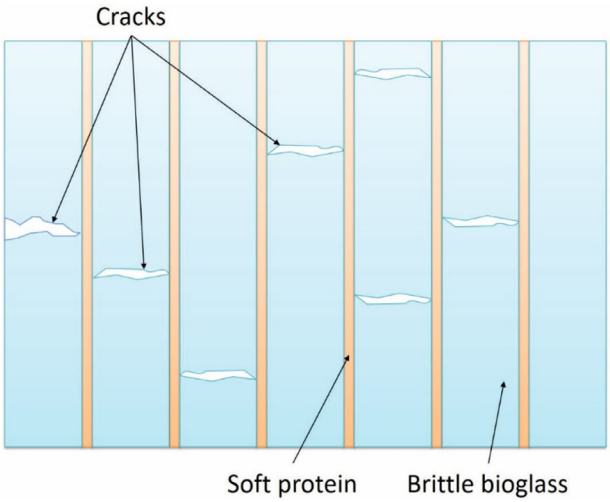

Fig. 2. Crack arrester effect in the skeleton of a deep-sea sponge due to the material inhomogeneity effect.

toughness. Literature such as Wu et al. (Wu et al., 2019) or Gu et al. (Gu et al., 2017) show, that interfacial strength and different layers of hierarchical structure also play an important role in replicating the excellent properties of natural materials. Unfortunately, the structure of nacre has limited potential for industrial applications at the moment. The complex, three-dimensional structure can thus far only be produced by 3D-inkjet printing (Jia et al., 2019; Jia and Wang 2019) or even more advanced manufacturing techniques, such as freeze casting or magnetically assisted additive manufacturing (Zhao et al., 2018; Mao et al., 2016; Yang et al., 2018). It should be noted, that the majority of commercially available monomer formulations for 3D-inkjet printing are acrylate- or methacrylate based photoreactive resins. The resulting polymers are commonly known to be inherently brittle and potentially harmful for human contact (Gorsche et al., 2016; Ligon-Auer et al., 2016; Friedman et al., 1965; Karalekas and Aggelopoulos 2003; Nylander-French and French 1998), with only a few exceptions (Oesterreicher et al., 2017; Oesterreicher et al., 2016b; Oesterreicher et al., 2016a; Mostegel et al., 2016; Oesterreicher et al., 2016c). Conventional processing techniques for thermoplastic polymers such as injection molding and extrusion are not known to produce nacre-like structures on a large scale yet. Therefore, the industrial use of these structures seems to be limited thus far for polymers.

The skeleton of the deep sea sponge *Euplectella aspergillum* features a microstructure, composed of alternating, concentric rings of bio-glass and soft protein (Figs. 1c and d) (Aizenberg et al., 2005). In comparison to nacre (Figs. 1a and b), neither the concept of platelet pullout and interlocking nor the mechanism of crack deflection can be used to explain its high fracture toughness. The increase in toughness is achieved by the well-designed sequence of soft and hard phases (Woesz et al., 2006; Kolednik et al., 2011). Therein, the layers of soft protein serve as crack-arresters and hinder growing cracks from causing catastrophic failure (Fig. 2).

Several studies have shown that this crack arrest occurs due to the so-called material-inhomogeneity effect (Kolednik et al., 2011; Kolednik 2000; Fratzl et al., 2007). The material inhomogeneity effect describes the influence of a material inhomogeneity on the magnitude of the crack driving force. All that is needed is an interface (IF), interlayer (IL) or even gradient between two materials with different mechanical properties such as elastic modulus E, yield stress σ_y or hardening exponent n. The effect of a material inhomogeneity on the crack driving force was already well known for linear elastic fracture

mechanics (Zak and Williams 1963; Cook and Erdogan 1972; Huajian 1991; Muju 2000; Fischer et al., 2012; Murali et al., 2011; Náhlík et al., 2010). Recent studies by Kolednik et al. (Kolednik et al., 2011; Simha et al., 2005; Simha et al., 2003) present a more general approach based on the configurational force concept (Maugin 1995; Gurtin 2000) and the *J*-integral *J* (Rice 1968) as driving force parameter. Therein, the far field *J*-integral J_{far} is a measure of the driving force induced in the entire specimen by the applied load (Kolednik et al., 2019). The *J*-integral close to the crack tip gives the crack driving force J_{tip}, whose magnitude determines whether a crack is able to propagate or not. For homogeneous hyperelastic materials, the *J*-integral is path-independent, which also means $J_{tip} = J_{far}$. When considering inhomogeneous materials, such as a bimaterial specimen with a single interface, the *J*-integral becomes path-dependent and J_{tip} differs from J_{far} in the form, $J_{tip} = J_{far} + C_{inh}$ (Kolednik et al., 2011; Simha et al., 2005; Simha et al., 2003). The parameter C_{inh} is denominated as material inhomogeneity term.

The main factor influencing C_{inh} is the mismatch in mechanical material parameters, such as σ_y, E or the introduced work until the yield point (Lach et al., 2017; Lach et al., 2014; Lach et al., 2016; Grellmann and Langer 2017). If a crack propagates from a hard to a soft phase, the material inhomogeneity term C_{inh} is positive and increases J_{tip}, which is referred to as anti-shielding effect. Compared to a crack propagating only in one phase, this will lead to a higher crack growth rate. Vice versa, for crack propagation from soft to hard phase, C_{inh} becomes negative and decreases J_{tip} in the process, also known as shielding-effect. In this case, a crack will grow slower or even arrest, since it requires a higher applied load in order to propagate than in a homogeneous phase.

An interlayer can be regarded as two consecutive interfaces, and the inhomogeneity terms for the first and second interface C_{inh1} and C_{inh2} can be summed up in the interlayer inhomogeneity term C_{IL}, as shown in Eqn 1 (Sistaninia and Kolednik 2014),

$$J_{tip} = J_{far} + C_{inh1} + C_{inh2} = J_{far} + C_{IL}. \quad (1)$$

By the introduction of a soft interlayer in a brittle matrix material, the anti-shielding and shielding effects at two interfaces are combined (Sistaninia and Kolednik 2014), see Fig. 3. An exemplary evolution of J_{tip} as a function of the distance between the interlayer and the crack tip L_1 is depicted in Fig. 3b. Therein, a soft interlayer with an elastic modulus of E_{IL} was introduced to a stiff and brittle matrix with an elastic modulus of E_{Matrix}. The curve shows a local minimum at the second interface. By utilizing this effect, a crack trap can be tailored. To overcome such a soft interlayer, the macroscopic loading parameter J_{far} has to be increased substantially, leading to an improvement in fracture toughness. For the deep sea sponge itself (Kolednik et al., 2011), as well as for several metallic and ceramic materials (Fratzl et al., 2007; Kolednik et al., 2019; Sistaninia and Kolednik 2014; Chen et al., 2007; Müller et al., 2009; Kolednik et al., 2010; Zechner and Kolednik 2013), this shielding and anti-shielding effects could be experimentally proven. Lach et al. (Lach et al., 2014) observed the influence of a material inhomogeneity on cracks growing towards the interface of polymeric bimaterials. While Lach et al. mainly focused on cracks growing towards an interface, the current work focuses on cracks growing to and beyond interlayers of soft material. Therefore, the approach of fracture toughness increase via multi-layer build ups seems promising. However, studies on its effectivity on polymers are still missing.

Polymeric layered structures can be produced by extrusion, or in this case co-extrusion in an efficient manner. Therefore, layered structures appear to be a potent candidate for biomimetic toughness enhanced composites, which could also be used at an industrial scale. Within the scope of this paper co-extruded, thermoplastic multi-layer composites are examined with regard to their fracture toughness increase by introducing soft interlayers and different ratios of mechanical properties.

2. Experimental

2.1. Materials

Since the material inhomogeneity effect relies on a significant mismatch in mechanical properties, a portfolio of materials with vastly different mechanical behavior should be examined. However, good adhesion between individual layers should also be ensured to avoid delamination at the interfaces.

For industrial applications, the use of highly mineral reinforced polymers is appealing. Mineral fillers cause a high stiffness and promote enhanced creep resistance. Furthermore, mineral based fillers are commercially available at a fraction of the price of the polymer matrix. Therefore, four different variations of polypropylene were used in this study. Two polypropylene compounds with different amounts of mineral filler were used as stiff and brittle matrix materials (moderately talcum particle reinforced (PP-MR) and highly reinforced (PP-HR)). For the soft interlayer a standard grade of polypropylene (PP) and a very compliant type of modified PP (PP-S) were used. The exact formulations of used materials are confidential and cannot be disclosed at this time.

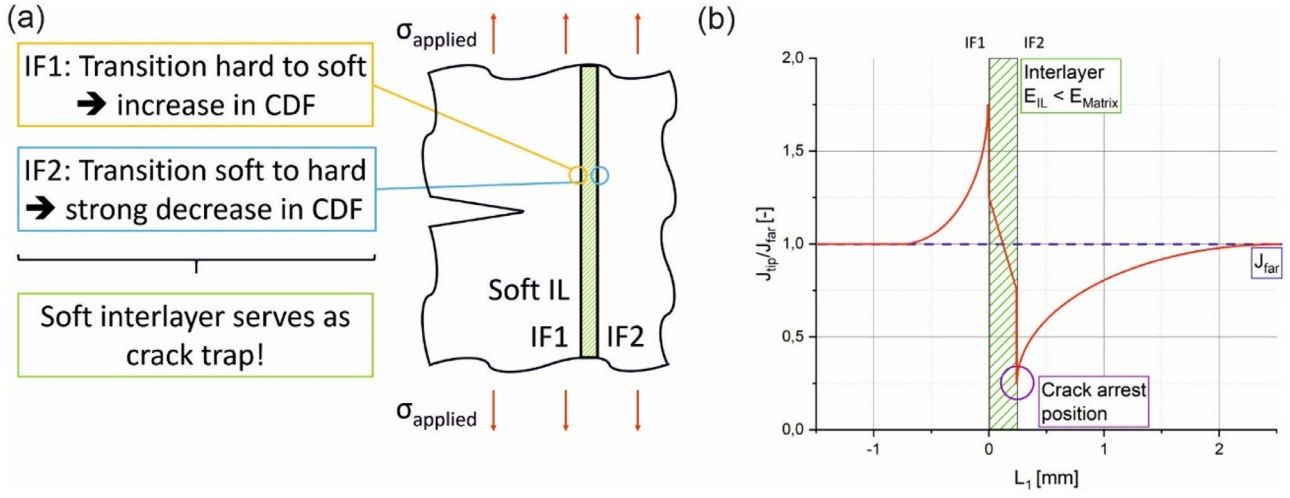

Fig. 3. Basic concept of creating a crack trap utilizing the material inhomogeneity effect (a) and the resulting change of J_{tip} in the vicinity of a soft interlayer (b) (Sistaninia and Kolednik 2014).

Table 1
Nomenclature and material composition for various multilayer configurations.

Abbreviation	Materials		number of interlayers	Ratio of mechanical properties		
	Matrix	Interlayer		E_{Matrix} / E_{IL}	σ_Y^M / σ_Y^{IL}	ε_f^M / ε_f^{IL}
ML1	PP-HR	PP	1	4.8	1.1	2.6×10^{-3}
ML2	PP-HR	PP-S	1	28.8	3.4	1.8×10^{-3}
ML3	PP-MR	PP-S	1	18.4	3.3	69.8×10^{-3}
ML4	PP-HR	PP-S	2	28.8	3.4	1.8×10^{-3}

2.1.1. Manufacturing of multi-layer composites

Using aforementioned materials, four different multi-layer composites (ML) were manufactured. The specific material combinations for matrix and interlayer, as well as the ratios of mechanical properties (respective values of matrix and interlayer for elastic modulus, E_{Matrix} and E_{IL}, yield stress,σ_Y^M and σ_Y^{IL}, and failure strains,ε_f^M and ε_f^{IL}) between them are shown in Table 1. Therein, ML1 has a PP-HR matrix with a single PP interlayer. In this combination, the ratios of mechanical properties are comparably low. In ML2, PP-S was used as single interlayer in a PP-HR matrix, leading to higher ratios of mechanical properties. ML3 has a single PP-S interlayer incorporated in a PP-MR matrix to observe the effects of a comparably tough matrix with a high mismatch in mechanical properties. ML4 has the same combination of materials as ML2, but features two interlayers. Using a co-extrusion process, homogeneous and multi-layered sheets with 20 mm thickness were produced. The average thickness of the soft interlayers was approximately 0.3 mm.

2.2. Fracture toughness testing using J-integral

Due to their ductile nature, three of the four investigated PP types do not comply with the assumptions made in linear elastic fracture mechanics. Therefore, methods of elastic plastic fracture mechanics are used to more accurately describe the material behavior of the multilayer specimens. More precisely, an adaptation of Rice's *J*-integral (Rice 1968; Hale and Ramsteiner 2001) method for polymers was utilized to characterize the fracture toughness. In accordance with the recommendation of the Technical Committee 4 of the European Structural Integrity Society (ESIS TC4 recommendation (Hale and Ramsteiner 2001)), the multi-specimen method using monotonic three point bending tests were performed on single edge notched bending (SENB) specimens.

From the (co-)extruded sheets, SENB specimens with the dimensions $80 \times 10 \times 20\,mm^3$ were produced (see Fig. 4). The longitudinal axis always coincided with the extrusion direction and the thickness of the sheet was taken as width of specimens (W). Machined notches were introduced and sharpened utilizing a broaching tool with a razor blade in order to produce an initial sharp crack with the length a_0 (Martínez et al., 2013; Martínez et al., 2016; Salazar et al., 2015). The initial notch lengths were manufactured to satisfy the relation $0.55 < a_0/W < 0.65$, as stated in (Hale and Ramsteiner 2001).

SENB tests (see Fig. 4b) were performed on the servo-hydraulic testing machine MTS 831 (MTS Systems GmbH, USA) at a crosshead speed of 1 mm/min. After performing the SENB experiments, the specimens were cryo-fractured and examined under a light microscope. An Olympus SZX12 (Olympus Life Science Europe GmbH, Germany) was used to obtain the crack extension, Δa, alongside the geometry data of the specimen under reflected light. To obtain the specimen thickness B and the ligament length W-a_0, three separate measurements were taken across the fracture area and averaged. A polygon was positioned to match the fractured surface and to calculate the fracture surface area. The average crack extension was calculated from the fracture surface area and B. For these measurements, a magnification of 12.5 was used in all cases. A preliminary *J*-integral, J_0 (which does not consider crack extension), was evaluated using Eq. (2).

$$J_0 = \frac{\eta U}{B(W - a_0)} \tag{2}$$

Therein, U is the area under the load-displacement curve, which was corrected for indentation and machine stiffness as stated in (Hale and Ramsteiner 2001). A value of 2 was used as geometry factor η for SENB specimens. Strictly speaking, the *J*-integral is only valid for very small crack extensions. To clearly observe fracture behavior before and after the interlayer, specimens had to be tested up to crack lengths of several mm. A crack growth correction according to (Schwalbe and Neale 1995) was performed to compensate for large Δa values. The experimental *J*-integral J_{exp} was then calculated using Eq. (3).

$$J_{exp} = J_0{}^*\left[1 - \frac{(0.75\eta - 1)\Delta a}{W - a_0}\right] \tag{3}$$

As is recommended by ESIS TC4 (Hale and Ramsteiner 2001), a power law fit was applied to the data of the four homogeneous materials. The power law formula is displayed in Eq. (4), wherein J_{exp} can be calculated from Δa and the two parameters A and N. All the gathered data can then be presented in a plot of J_{exp} against Δa, also known as *J*-*R* curve.

$$J_{exp} = A\ \Delta a^N \tag{4}$$

Following the procedure described in (Hale and Ramsteiner 2001) a so-called blunting line was constructed. This line follows the equation

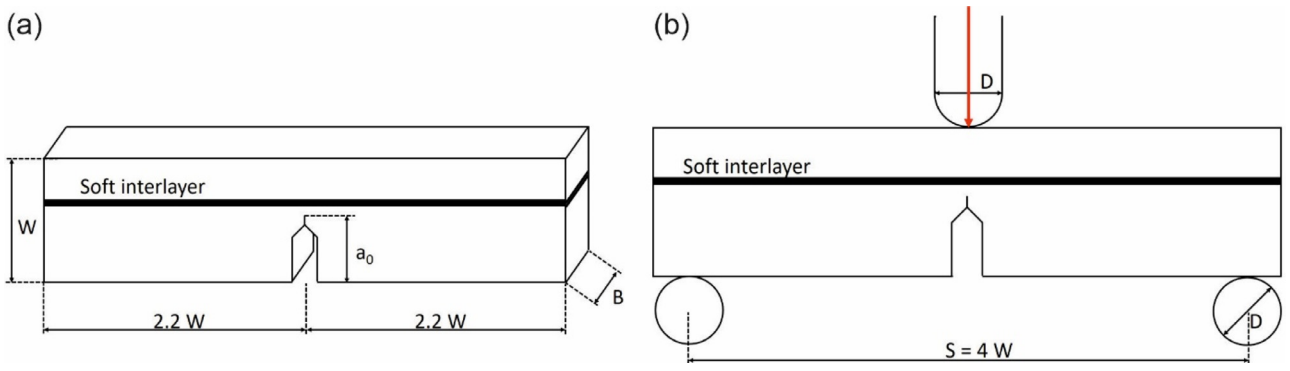

Fig. 4. Dimensions of a SENB specimen (a) and schematic of a bending fixture (b) (Hale and Ramsteiner 2001).

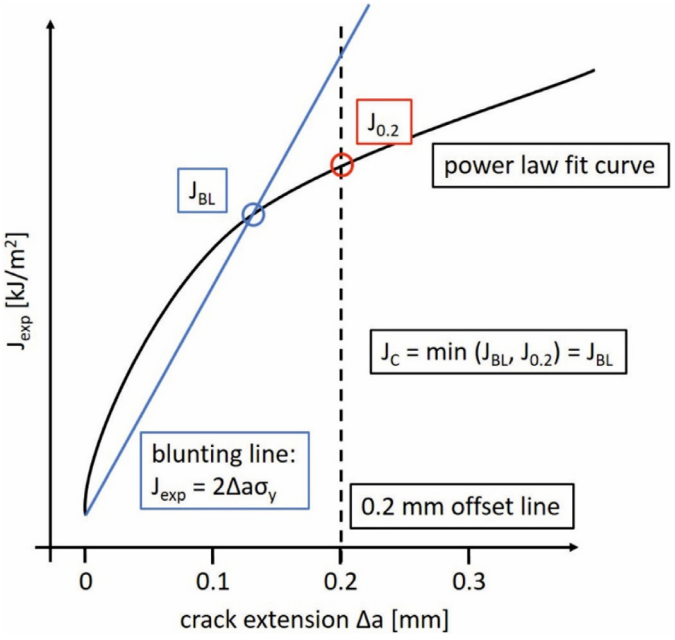

Fig. 5. Determination of J_C from J_{BL} and $J_{0.2}$.

$J_{exp} = 2\Delta a\sigma_y$ and describes the crack tip blunting due to plastic deformation. The intersection of the blunting line with the power law fit curve yields the parameter J_{BL}. The power law fit formula was used to evaluate the J_{exp} value at $\Delta a = 0.2$ mm in order to obtain the value $J_{0.2}$. The initiation toughness parameter J_C was then determined as the smaller value out of J_{BL} and $J_{0.2}$, see Fig. 5.

As shown in several works before, PP shows a rather complex deformation mechanism in fracture mechanical tests whether it is under monotonic (Salazar et al., 2014; Seidler et al., 2001), impact (Martínez et al., 2016; Salazar et al., 2012; Karger-Kocsis et al., 1997), or fatigue (Arbeiter et al., 2016) loading. Thus, a certain amount of data scattering is also expected for the materials at hand. A simple criterion was applied to discard specimens with unstable crack growth to ensure adequate quality of data points in the *J-R* curve (Lach et al., 2014; Gosch et al., 2018). A linear regression line was fitted to the crack growth Δa versus testing time *t*. Very far outliers from the trend line were excluded from the evaluation. When introducing interlayers a change of the crack growth rate in the vicinity of the soft layer is expected. Hence, this data exclusion criterion was only applied for homogeneous materials and not for multi-layer configurations.

2.3. Adaptations of Δa-measurement and J-Rplotting technique for materials with interlayers

Due to the complex fracture process of inhomogeneous materials, the conventional methods for crack length measurement and construction of the *J-R* curve have to be adapted. Presumably, owing to the interlayer material's high failure strain, the interlayer itself stays intact during the experiment and does not break until the specimens are cryo-fractured. Therefore the interlayer thickness, t, was never included in the crack extension Δa. Instead, the individual crack extensions Δa_i in the matrix material were added up to a total Δa. In the case of a single interlayer this leads to $\Delta a = \Delta a_1 + \Delta a_2$ (see Fig. 6a).

Another aspect in multi-layered specimens is that many geometrical parameters are subject to variance related to processing and sample preparation. While the differences may seem small compared to the dimensions of the specimen, even small changes can have a significant influence on the *J-R* curve. Processing induced variances, such as the distance between the interlayer and the razor blade notch L_0, the interlayer thickness *t* or the remaining ligament behind the interlayer can lead to large scatter in the J_{exp} values at the first interface of the interlayer.

To compensate for these variances in geometry, an alternative technique of plotting is used. Instead of applying J_{exp} versus the crack extension Δa, a parameter *L* was introduced as replacement for Δa (Fig. 6a).The parameter *L* describes the distance between the first interface of the soft layer and the crack tip. A negative value of *L* indicates that the crack has not reached the interlayer yet. In this case $L = \Delta a\text{-}L_0 < 0$ (see Fig. 6a). In contrast, positive values indicate crack growth beyond the interlayer. In the case of a single interlayer, this means $L = \Delta a\text{-}L_0 = \Delta a_2 > 0$. As a result, effects caused by the material inhomogeneity should be clearly visible at or closely around a value of $L = 0$ (Figs. 6b and c).

For the multi-layer composites, a linear regression line for all data points with $L > 0$ was fitted and extrapolated to $L = 0$ (see Fig. 6c). This intersection represents the required energy to overcome the interlayer and initiate crack growth behind it. The obtained value was named J_C^{ML} and served as a measure for the fracture toughness of the composite. The slope of the regression line is proportional to the tearing modulus *T* ($T = E/\sigma_y^2 * dJ_{exp}/d(\Delta a)$). Although *T* is known to be geometry dependent, the slope $dJ_{exp}/d(\Delta a)$ shall be used to qualitatively compare the crack growth resistance.

For better comparison, a shifting procedure was also applied for the *J-R* curves and Δa-*t* plots (crack extension versus testing time) of the matrix materials. The arithmetic mean of L_0 was calculated from all specimens of the individual multi-layer configurations (e.g. L_0^{ML1}, L_0^{ML3}). The data points and power law fit curves of the respective matrix materials PP-HR and PP-MR were shifted by these values, so that $L_{matrix} = a_{matrix} - L_0^{ML}$. By formulating the parameter *L* as mentioned, the *J-L* plot can describe the J_{exp} behavior for both homogeneous as well as multi-layered specimens. This does not influence the representation of the *J-R* curve as well as the *L-t* curve of the homogeneous specimens.

3. Results & discussion

3.1. Fracture toughness of homogeneous materials

For all specimens made from PP and PP-S, side grooves with a depth equal to 10% of the thickness *B* were introduced on each side. This was done to avoid strong curvatures of the crack fronts during the experiments. For PP-HR and PP-MR specimens side grooves were applied only to a part of the specimens that were tested. Fracture mechanical SENB tests could successfully be performed for three out of the four homogeneous materials (PP, PP-MR and PP-HR). The resulting *J-R* curves are depicted in Fig. 7. The obtained values for the constants A and N of the power law fit (Eq. (4)) as well as the values for $J_{0.2}$, J_{BL} and J_C are shown in Table 2. One material, namely PP-S, was too ductile to be characterized via *J*-integral at room temperature. During testing the specimens just plastically deformed instead of fracturing. Even at very large deflections, no actual crack extension from the initial razor blade notch could be detected. Additionally, PP showed a great discrepancy between J_{BL} and $J_{0.2}$ (19.32 kJ/m^2 and 44.59 kJ/m^2), making a reliable determination of fracture toughness somewhat difficult. Alternative techniques for determining the initiation toughness parameter include assessment of stretched zone width and height, crack tip opening displacement (CTOD, often used for metals e.g. (Kolednik et al., 2019)) or even the kinetics of the CTOD. (Lach and Grellmann 2017; Lach et al., 2005) However, due to the unreliable measurement of CTOD in polymers at low speeds these methods were forgone in the current contribution. Owing to the higher degree of mineral reinforcement, a reduction in J_C could be observed for PP-HR in comparison to PP-MR (0.23 kJ/m^2 compared to 1.30 kJ/m^2). Interestingly, for PP-MR and PP-HR no difference between side grooved and non-side grooved specimens could be observed. Contrary to ESIS TC4 recommendation, *J-R* curves were measured up to rather large values of crack extension, to

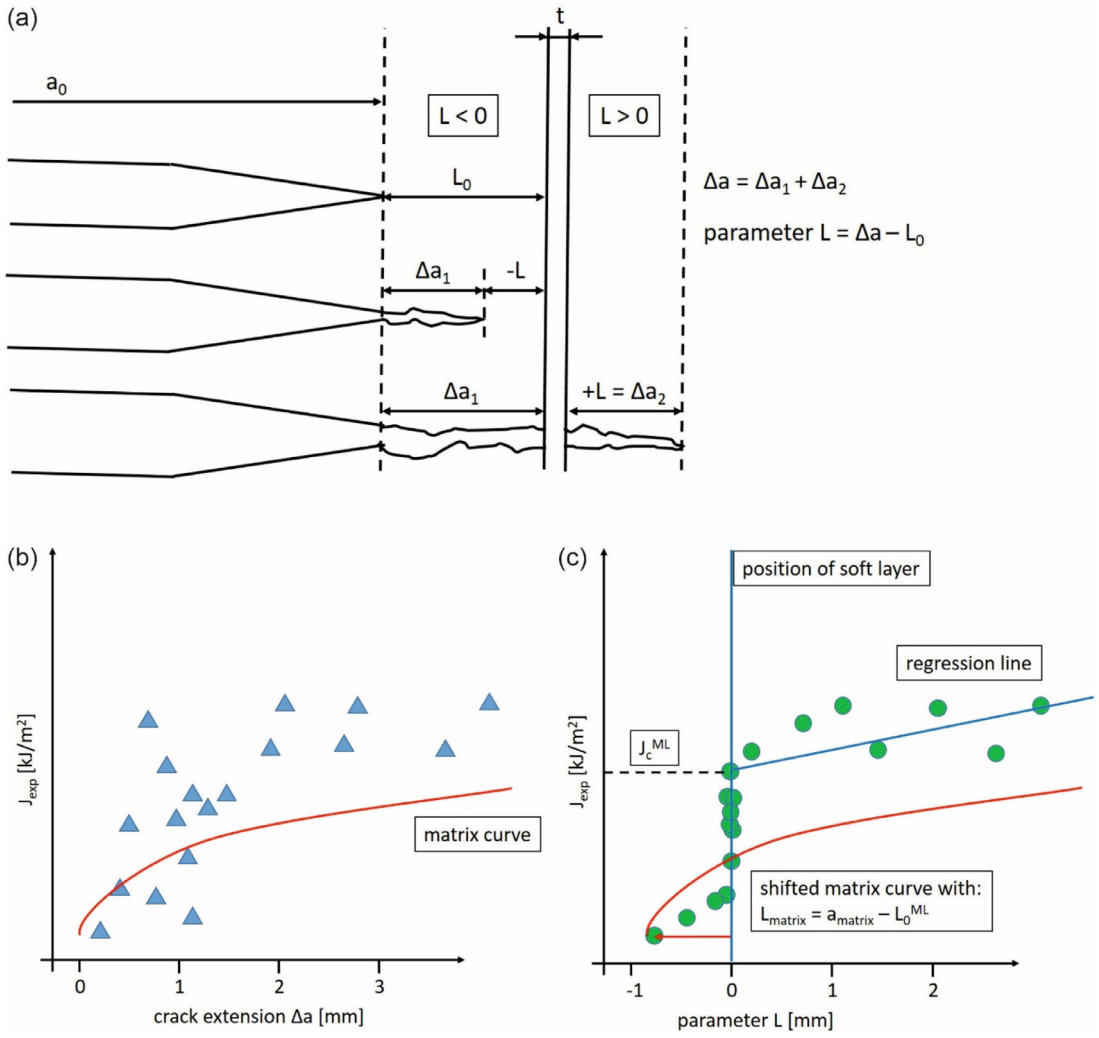

Fig. 6. Calculation of the parameter L (a), conventional plotting of J_{exp} versus Δa (b) and modified plotting technique (c) of J_{exp} versus the distance between crack tip and interlayer (parameter L).

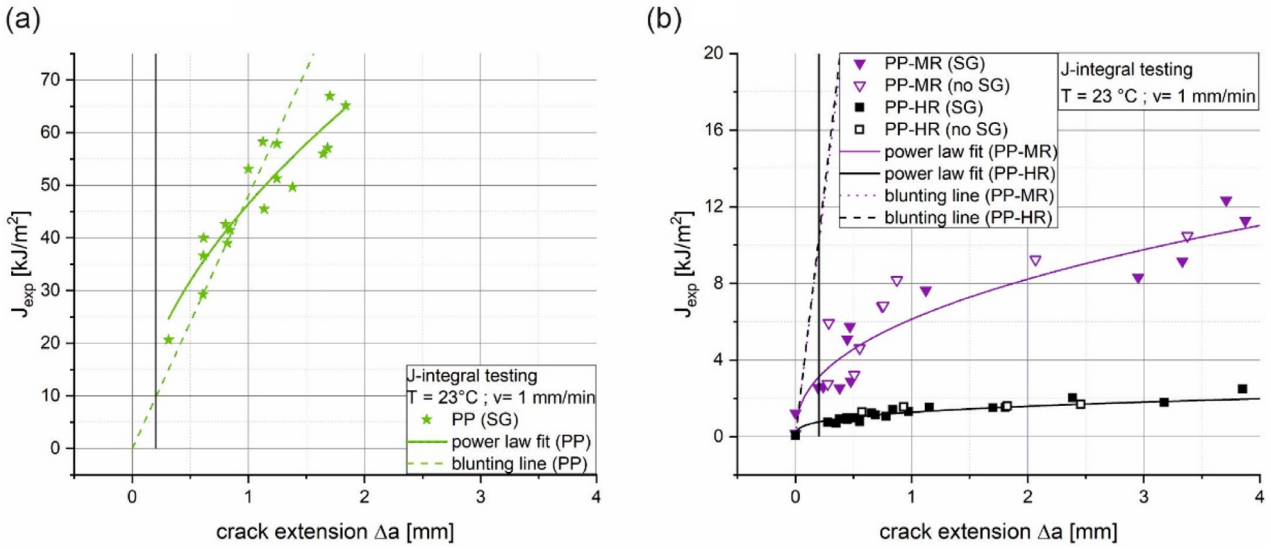

Fig. 7. *J-R* curve for PP (a), PP-MR (b) and PP-HR (b), tested at a crosshead speed of 1 mm/min. Measurement points, power law fits as well as blunting lines are shown.

Table 2
Overview of and power law fit parameters for Eq. (4), A and N, and fracture toughness parameters $J_{0.2}$, J_{BL}, J_C and J_C^{ML} for the tested materials.

homogeneous materials						multi-layer composites (non-side grooved)	
	A	N	$J_{0.2}$ [kJ/m^2]	J_{BL} [kJ/m^2]	J_C [kJ/m^2]		J_C^{ML} [kJ/m^2]
PP	46.43	0.55	19.32	44.59	19.32	ML1	–
PP-S	–	–	–	–	–	ML2	1.94
PP-MR	6.26	0.41	2.60	1.30	1.30	ML3	24.07
PP-HR	1.27	0.32	0.76	0.23	0.23	ML4	2.42

compare with multi-layer specimens later on.

3.2. Fracture toughness of composites

3.2.1. Multi-layer composite 1 (ML1; matrix: PP-HR; interlayer: PP)

For ML1 specimens side grooves with a depth equal to 10% of B were applied only to a part of the specimens that were tested. The results for ML1 are shown in Fig. 8. Although ML1 contains a comparably tough PP interlayer, no improvements in fracture initiation toughness or crack growth resistance could be achieved compared to pure PP-HR. For non-side grooved specimens the J_{exp}-values are slightly below the matrix material, while the crack growth rate is higher (0.168 mm/s compared to 0.084 mm/s, see Figs. 8a and b). Due to the high constraint caused by the surrounding matrix and the resulting stress triaxiality, the plasticity of the PP interlayer is limited. Although some plastic deformation takes place, no energy consuming large scale yielding is observed. The significant attribute for the toughening of the composite is the inhomogeneity effect, which also affects the crack driving force and stress distribution in matrix regions adjacent to the interlayer. While the ratio of E between the two materials is significant, the same cannot be said for the ratio of σ_y. The yield stress of the matrix is only 10% higher than that of the interlayer. This E-inhomogeneity will be diminished by plastic deformation near the interfaces. As described in (Kolednik et al., 2019), this results in a strongly reduced effectiveness of the interlayer as crack arrester. Hence, the combined inhomogeneity effect ($E + \sigma_y$) is not strong enough to cause a measurable increase in fracture toughness. This would not be so in the case of σ_y-inhomogeneity, whereas the ideal scenario is an inhomogeneity in both E and σ_y. The side grooved specimens coincide with the matrix material PP-HR in both the J-R curve and the crack growth rate. For that reason, no initiation parameter J_C^{ML} was evaluated.

3.2.2. Multi-layer composite 2 (ML2; matrix: PP-HR; interlayer: PP-S)

For ML2 specimens side grooves with a depth equal to 10% of B were applied only to a part of the specimens that were tested. In ML2, the differences of σ_y and E between matrix and interlayer materials are much higher than in ML1. As a result, the ML2 composite shows an E-inhomogeneity as well as a σ_y-inhomogeneity. Hence, the combined inhomogeneity effect should show a greater influence on the fracture toughness. For all the non-side grooved specimens the soft interlayer noticeably influenced the crack growth behavior (see Figs. 9a and b). For ML2, an increase from 0.23 kJ/m^2 (J_C of the PP-HR matrix) to 1.94 kJ/m^2 (J_C^{ML2} of the composite, see Table 2) could be achieved.

The slope of J-R curve, $dJ/d(\Delta a)$, is different in the region $L<0$, for PP-HR and its composites. The predicted anti-shielding effect becomes visible, since the slope of 0.31 kJ/m^3 for $L<0$ is visibly lower than for pure PP-HR. When the crack reaches the interlayer, this slope almost becomes a vertical line. The energy for plastic deformation and crack re-initiation behind the interlayer must be overcome first, before another increment of crack extension can be produced. Thereafter, the $dJ_{exp}/d(\Delta a)$ of ML2 is lower than for the matrix PP-HR, 0.18 kJ/m^3 compared to 0.28 kJ/m^3. This might be due to a change in constraint (a/W) and possibly the release of elastically stored energy as additional source of crack driving force.

For $L<0$, the crack growth rate at 0.055 mm/s was found to be slighltly below the matrix value of 0.084 mm/s. The crack growth rate (evaluated as the slope in the L-t plot, Fig. 9b) almost drops to zero in the proximity of the interlayer. After passing the interlayer the crack growth rate increases to 0.137 mm/s compared to the 0.084 mm/s of PP-HR. As can be seen in Fig. 10a, PP-HR shows no signs of significant plastic deformation or yielding. The only trace of dissipative effects is a slim zone of stress whitening (possibly caused by crazing) that precedes the crack. While the crack is arrested in the interlayer but the loading continues, the majority of introduced energy has no other possibility than to be stored as elastic energy. Once a crack re-initiates in the matrix however, this energy is released again, resulting in an accelerated crack growth. This assumption is confirmed by the decreased slope in the J-R curve for $L>0$.

For the side-grooved specimens no improvement in fracture toughness could be achieved. The J_{exp}-values are even lower that for PP-HR, while the crack growth rate is higher than for the matrix (0.233 mm/s compared to 0.084 mm/s).

3.2.3. Multi-layer composite 3 (ML3; matrix: PP-MR; interlayer: PP-S)

None of the previously performed experiments showed improvements in fracture toughness when introducing side grooves. Therefore,

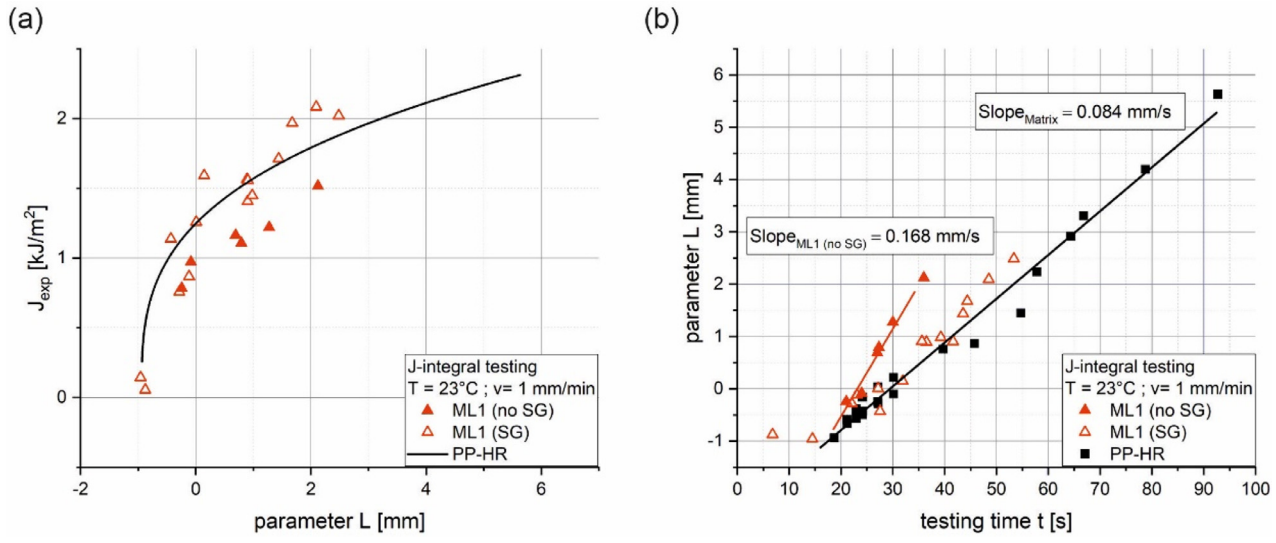

Fig. 8. Modified J-R curve for ML1 displaying J_{exp} versus the parameter L (a) and L versus testing time (b).

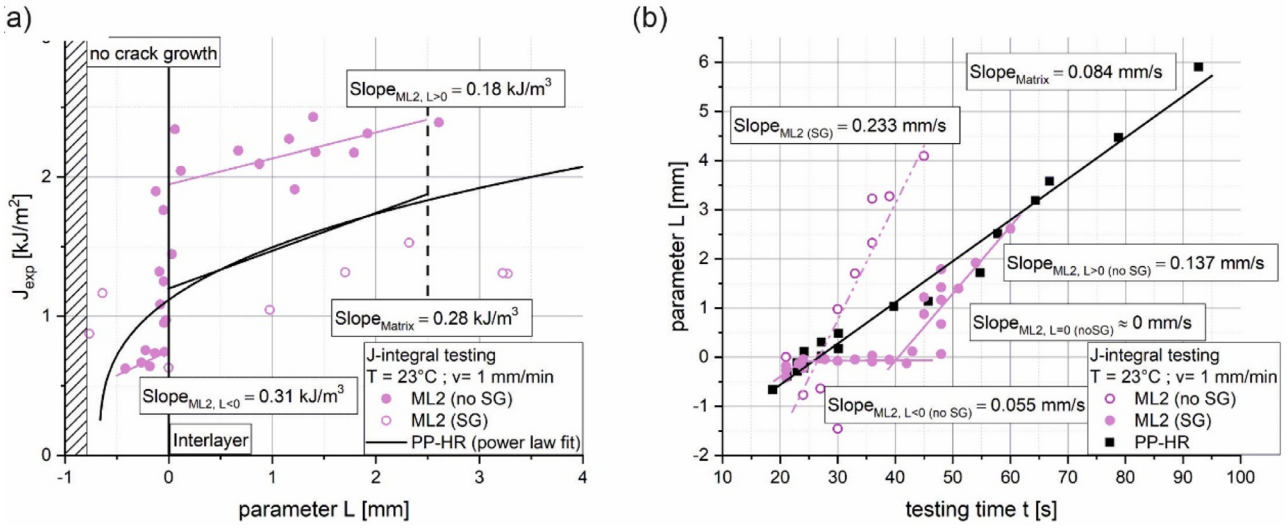

Fig. 9. Modified *J-R* curve for ML2 displaying J_{exp} versus the parameter L (a) and L versus testing time (b).

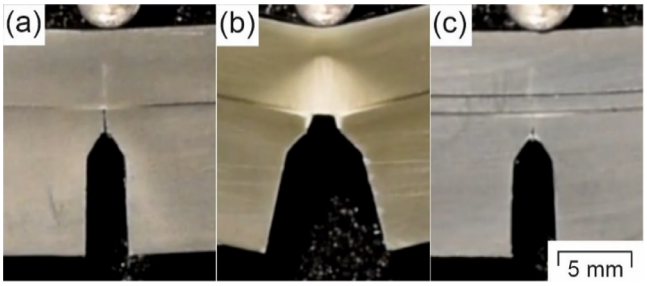

Fig. 10. Plastic zone development shortly before crack re-initiation for ML2 (a), ML3 (b) and ML4 (c).

side grooves were omitted entirely for ML3 specimens. A pronounced increase of J_{exp} can be seen at $L = 0$ for ML3 specimens (Fig. 11a). The increase for ML3 is considerably higher than for ML2. More precicely, the fracture toughness at $L = 0$ increased almost twenty times from 1.30 kJ/m^2 (J_C of PP-MR) to 24.07 kJ/m^2 (J_C^{ML3} of ML3, see Table 2). This is caused by the tougher matrix material, which hinders crack re-initiation after the first crack hits the interface. What is also worth mentioning is the increased slope of 11.37 kJ/m^3 for $L > 0$ as compared to 1.66 kJ/m^3 of PP-MR. Apparently, the crack growth resistance after passing the interlayer is higher than for the pure matrix. This is possibly caused by the extensive plastic deformation the remaining ligament undergoes before crack re-initiation. Therefore, higher amounts of dissipated energy are required for further crack extension. The possibility to express this in the form of J_{exp} should be taken with care due to invalidation of *J*-integral preconditions. Furthermore, PP-MR is able to undergo a strain softening process without fracture when being loaded past σ_y. This process is comparable to the mechanical rejuvenation effect described by Meijer and Govaert (Meijer and Govaert 2005). Therefore, the applied strains can be delocalized better, while crazing becomes less likely. As a result, the plastically deformed material shows an increase in fracture toughness compared to its undamaged state.

For $L < 0$ cracks propagate a lot faster than in pure matrix material. This behavior can be explained by the variation of crack driving force around the interlayer, which is depicted in Fig. 2b. While the crack driving force behind the soft layer is diminished by the shielding effect, in front of the interlayer the anti-shielding effect leads to an increased

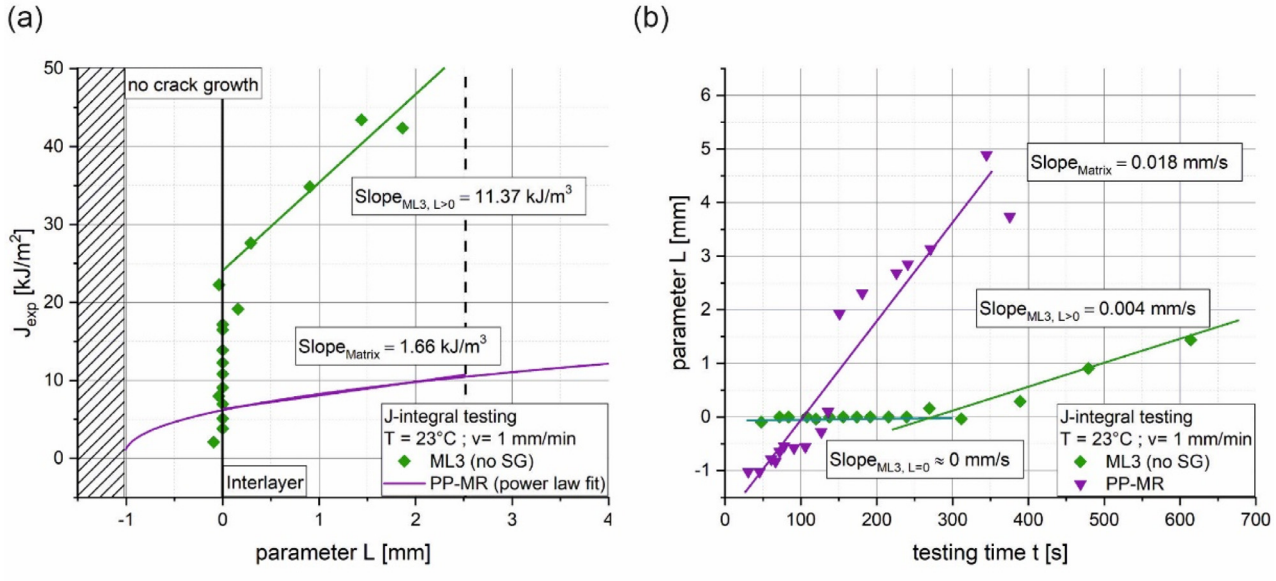

Fig. 11. Modified *J-R* curve for ML3 displaying J_{exp} versus L (a) and L versus testing time (b).

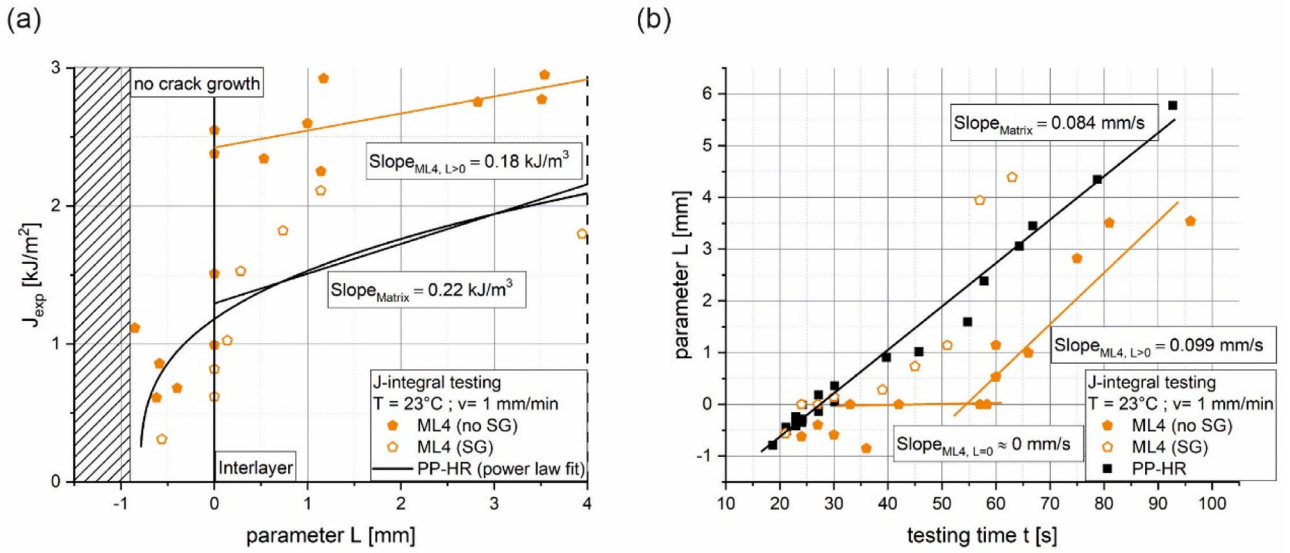

Fig. 12. Modified *J-R* curve for ML4 displaying J_{exp} versus the parameter L (a) and L versus testing time (b).

crack driving force and crack growth rate. This can also be seen in Fig. 11b, where almost 1 mm of crack extension is reached very rapidly. Smaller crack extensions could not be measured within the scope of the experiments. However, after this fast crack propagation towards the interlayer the crack growth rate rapidly drops to zero upon reaching it. In accordance with the *J-R* curve, the crack growth rate for $L>0$ is much smaller than for undamaged PP-MR (0.004 mm/s compared to 0.018 mm/s). Once again this indicates tougher material behavior of the plastically deformed matrix material.

3.2.4. Multi-layer composite 4 (ML4; matrix: PP-HR; interlayer: PP-S)

For ML4 specimens side grooves with a depth equal to 10% of B were applied only to a part of the specimens that were tested. For non-side grooved specimens a tenfold increase from 0.23 kJ/m^2 to 2.42 kJ/m^2 in fracture toughness could be measured (see Table 2), although the data exhibited big scattering in the ML4 experiments.

The plot of L versus testing time in ML4 is similar to ML2. As is depicted in Fig. 12a, the slope in the *J-R* curve for $L>0$ is slightly smaller than for the matrix (0.18 kJ/m^3 compared to 0.22 kJ/m^3). The crack growth rate (Fig. 12b) almost drops to zero at $L = 0$. With 0.099 mm/s, the crack growth rate behind the interlayer is again larger than for PP-HR (0.084 mm/s), so that for large values of L the two curves join again. Due to the higher data scattering, no reliable statement can be made for the slope of the *J-R* curve and the slope in the L-t plot for $L<0$. Just as for ML2, the plastic zone of ML4 was found to be very small (Fig. 10c). The data points for side grooved specimens coincide with the matrix material. Despite what one would expect from a specimen with two interlayers, no second increase in J_{exp} was observed. This is explained by the unexpected failure mechanism, which will be discussed in the next section.

3.2.5. Specimen failure mechanism

Surprisingly, even after a crack has re-initiated beyond an interlayer, the interlayer still remains intact and endures large deformations until rupture (Fig. 6a). This observations was made for all four multi-layer configurations. For ML2, ML3 and ML4, the crack is stopped at $L = 0$ and has to re-initiate in the remaining matrix ligament, while for ML1 no such benefits were found. This raises the question which mechanism actually causes the final specimen failure. Fig. 13 depicts different scenarios for the fracture behavior of a SENB specimen with two soft interlayers. The consideration was made for two interlayers (corresponds to ML4) but the discussed failure mechanisms would look the same for a single interlayer composite. In both scenarios, the specimen is assumed to be already fractured from the initial notch until to the first soft interlayer. Fracture surface is depicted as grey area with black dots, the initial razor blade notch is depicted as white area with black stripes. While the interlayer itself (black area) stays intact, it is not sure where the specimen failure will proceed in the matrix material (white area with black spots). There are two plausible causes for crack re-initiation in the matrix behind the soft layer:

3.2.5.1. Scenario A: the interlayer transfers stresses in a meaningful way. The interlayer and matrix transfer the bending stress σ_b in the same way and the stress distribution is almost unaffected by the material inhomogeneity. Just as one would expect from a homogeneous sample, the highest stresses occur at the crack tip (Fig. 13a). However, the interlayer material is too tough to fail at this location. It is more likely that the interlayer stays intact and a new crack re-initiates in a part of the matrix closest to the arrested crack. In the depicted case, this would be the middle ligament of the SENB specimen.

3.2.5.2. Scenario B: the interlayer transfers no stresses. In this case, stress transfer from one ligament to the next is not possible. However, all ligaments have the same deflection. Thus, the ligaments behave like separate, decoupled bending specimens. Each individual ligament posseses its own bending stress distribution (Fig. 13b). Just like before, the interlayers are too tough to break and stop any growing cracks. Now the most critical stress can be found on the tension side of the broadest matrix ligament. For the depicted geometry, the maximum stress and therefore the location for crack re-initiation can be found on the bottom edge of the outermost matrix ligament. If the loading parameters are known, the fracture toughness of a structure can also be optimized. By using equally spaced, small ligaments, the maximum stress can be kept below the matrix material's bending strength (see Fig. 13b).

It should be noted that in both cases specimen failure does not progress through classical crack growth, but rather due to a surpassing of the matrix material strength at a global stress maximum. Any increment of crack extension behind the first soft layer can only happen after a crack re-initiation step.

In order to distinguish which one of the aforementioned failure mechanisms really happens, the fracture surfaces of cryo-fractured SENB specimens were investigated closer. Of course, in ML2 specimens (Fig. 14a and c) crack re-initiation happens behind the first and only interlayer. No differentiation between Scenario A and B can be made in

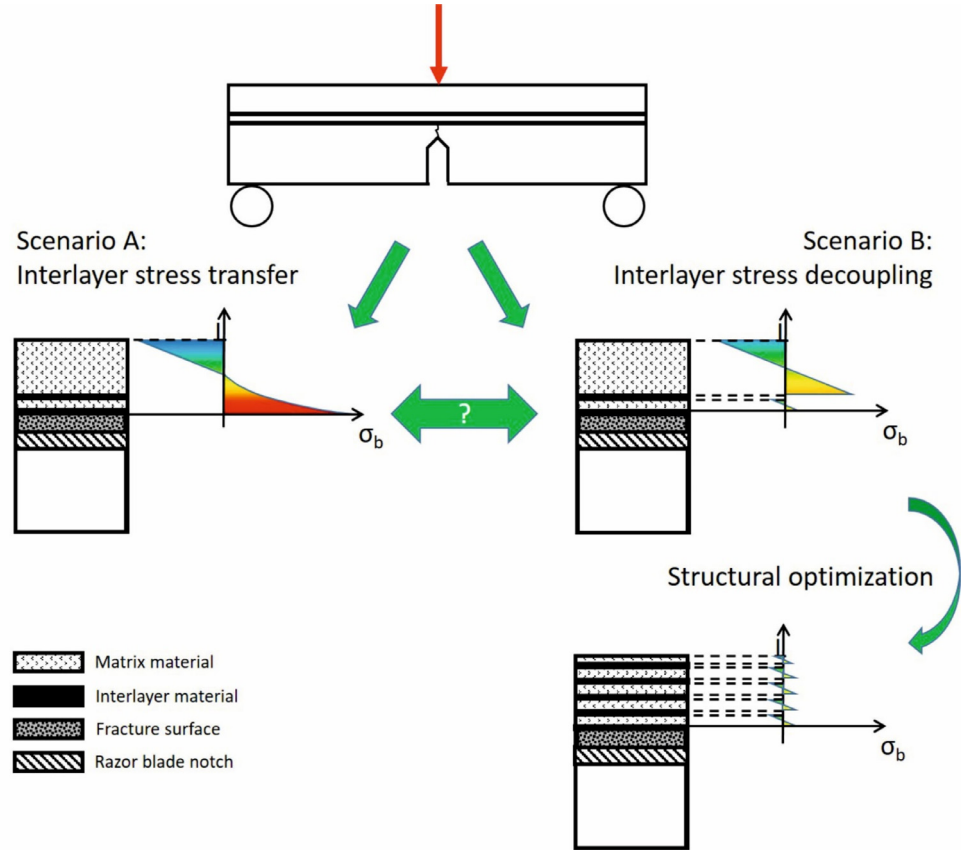

Fig. 13. Possible stress distributions in multi-layered specimens: interlayer is able to transfer stresses well (Scenario A) and interlayer transfers no stresses (Scenario B).

this case. However, fracture surfaces from ML4 specimens (Fig. 14b and d) are more revealing: While the middle ligament is still intact, crack re-initiation takes place in the outermost matrix ligament. The failure of the broadest ligament confirms the assumptions of decoupled bending stresses made in 3.2.5 b. Specimen failure in this case does not proceed consecutively from the first interlayer to the second, but rather due to a simultaneous loading of all deflected ligaments. This gives the explanation why there is no second increase in J_{exp} for ML4 in Fig. 12a.

In specimens with side grooves the crack re-initiation always started from the bottoms of the side grooves (Fig. 14a and b). For PP-HR the stress concentration introduced by the side grooves is significant enough to greatly facilitate crack re-initiation. In these cases, the side grooves render the introduction of soft layers obsolete. For this reason, no improvements in fracture toughness and crack growth rate could be found.

On the other hand, in the specimens without side grooves, the exact location of re-initiation behind the interlayers varried randomly (Fig. 14c and d). The starting points of failure are most likely local stress concentrations caused by agglomerates of mineral particles. All specimens failing in this way exhibited the increase in fracture toughness and crack growth rate predicted by the material inhomogeneity effect. In these cases, the soft layers worked as intended.

4. Summary & conclusions

Inspired by bio-materials, the effects of soft polymer interlayers on mineral reinforced polymer matrix materials were characterized. The improvements of fracture toughness caused by the soft layers were shown using *J*-integral-based methods from elastic plastic fracture mechanics. The following statements were found to be true in single edge notch bending tests:

- The material inhomogeneity effect was observed in mineral reinforced polypropylene (PP) with PP interlayers. Through the introduction of soft interlayers in brittle matrix materials, improvements in fracture toughness could be achieved due to a crack-arrester effect in the soft layers.
- In order to function as intended, the interlayer material must exhibit large differences in the elastic modulus E and the yield stress σ_y compared to the matrix material. The pure σ_y-inhomogeneity is more influential, while a pure E-inhomogeneity yielded no benefits due to plastic deformation at the interlayer. However, a combined inhomogeneity (E and σ_y) is ideal.
- Once a crack is arrested by a soft layer, specimen failure is determined by crack re-initiation in the matrix material. *Re*-initiation is influenced by matrix and interlayer material and will happen at the location of the highest stress.
  - For a moderately mineral reinforced PP matrix, the re-initiation step is difficult, leading to a big increase in fracture toughness .
  - Crack re-initiation is easier in a highly mineral reinforced PP matrix. This leads to a smaller improvement in fracture toughness by soft interlayers.
  - *Re*-initiation is difficult for an interlayer made of soft PP. No stress transfer was possible between the matrix ligaments, which then behaved like decoupled bending specimens.
  - An interlayer made of standard PP yielded no benefits in fracture toughness because the difference in σ_y compared to the matrix was too small.
  - The introduction of side grooves to the specimens also greatly facilitated crack re-initiation.
- In order to more clearly depict the influence of soft interlayers, a new plotting technique was developed. Therein, the experimental *J*-integral J_{exp} is plotted against the newly defined parameter L. From

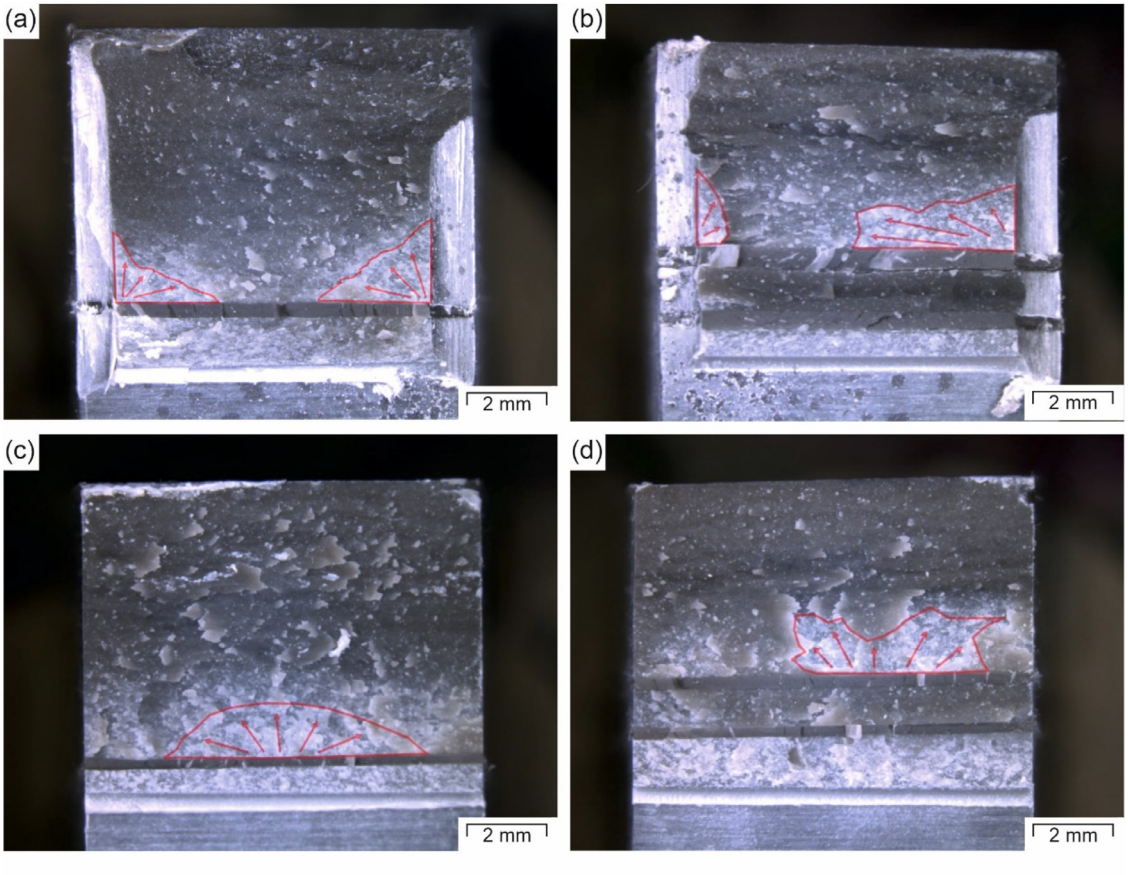

Fig. 14. Fracture surfaces of side grooved ML2 (a), side grooved ML4 (b), non-side grooved ML2 (c) and non-side grooved ML4 specimens (d). Crack re-initiation is indicated with red arrows.

these *J-L* plots, a fracture toughness for multi-layer composites, J_C^{ML}, could be determined.

In future work the influences of interlayer thickness, interlayer position and number of interlayers should be investigated. A full understanding of all influencing factors and their interactions has not been reached yet. The next task would be properly defining material laws, which quantitatively describe not only the crack growth, but also the re-initiation step. With these issues solved, analyzing structures with the help of FE methods could be attempted, yielding a most useful tool for structural optimization in multi-phase composites.

Declaration of Competing Interest

The authors declare that they have no known competing financial interests or personal relationships that could have appeared to influence the work reported in this paper.

Acknowledgements

This research was supported by the Austrian Research Promotion Agency (FFG) as part of the project “Entwicklung und Optimierung von hoch risszähen, polymeren Mehrschicht-Verbundsystemen nach biomimetischen Prinzipien”, grant agreement 858562, referred to with the acronym “BioMimicPolymers“. Special thanks go to Franz Grassegger and Nina Hochrainer for the diligent preparation of the test specimens, to Jürgen Grosser for his competent support with testing infrastructure and Anja Gosch for fruitful discussions regarding elastic plastic fracture mechanics.

Supplementary materials

Supplementary material associated with this article can be found, in the online version, at doi:10.1016/j.mechmat.2019.103243.

References

Aizenberg, J., Weaver, J.C., Thanawala, M.S., Sundar, V.C., Morse, D.E., Fratzl, P., 2005. Skeleton of euplectella sp.: structural hierarchy from the nanoscale to the macroscale. Science 309 (5732), 275–278. https://doi.org/10.1126/science.1112255.

Arbeiter, F.J., Frank, A., Pinter, G., 2016. Influence of molecular structure and reinforcement on fatigue behavior of tough polypropylene materials. J. Appl. Polym. Sci. 133 (38), 1237. https://doi.org/10.1002/app.43948.

Ashby, M., Cebon, D., 1993. Materials selection in mechanical design. J. Phys. IV France 03 (C7) C7-1-C7-9. https://doi.org/10.1051/jp4:1993701.

Barthelat, F., Espinosa, H.D., 2007. An experimental investigation of deformation and fracture of nacre–mother of pearl. Exp. Mech. 47 (3), 311–324. https://doi.org/10.1007/s11340-007-9040-1.

Chen, C., Pascual, J., Fischer, F., Kolednik, O., Danzer, R., 2007. Prediction of the fracture toughness of a ceramic multilayer composite – Modeling and experiments. Acta. Mat. 55 (2), 409–421. https://doi.org/10.1016/j.actamat.2006.07.046.

Cook, T.S., Erdogan, F., 1972. Stresses in bonded materials with a crack perpendicular to the interface. Int. J. Eng. Sci. 10 (8), 677–697. https://doi.org/10.1016/0020-7225(72)90063-8.

Dutta, A., Tekalur, S.A., 2014. Crack tortuousity in the nacreous layer – Topological dependence and biomimetic design guideline. Int. J. Solids Struct. (International Journal of Solids and Structures) 51 (2), 325–335. https://doi.org/10.1016/j.ijsolstr.2013.10.006.

Dutta, A., Tekalur, S.A., Miklavcic, M., 2013. Optimal overlap length in staggered architecture composites under dynamic loading conditions. J. Mech. Phys. Solids 61 (1), 145–160. https://doi.org/10.1016/j.jmps.2012.08.005.

Fischer, F.D., Predan, J., Fratzl, P., Kolednik, O., 2012. Semi-analytical approaches to assess the crack driving force in periodically heterogeneous elastic materials. Int. J. Fract. 173 (1), 57–70. https://doi.org/10.1007/s10704-011-9657-z.

Fratzl, P., Gupta, H.S., Fischer, F.D., Kolednik, O., 2007. Hindered crack propagation in materials with periodically varying young's modulus—lessons from biological materials. Adv. Mater. 19 (18), 2657–2661. https://doi.org/10.1002/adma.200602394.

Friedman, M., Cavins, J.F., Wall, J.S., 1965. Relative nucleophilic reactivities of amino groups and mercaptide ions in addition reactions with α,β-Unsaturated compounds 1,2. J. Am. Chem. Soc. 87 (16), 3672–3682. https://doi.org/10.1021/ja01094a025.

Gorsche, C., Seidler, K., Knaack, P., Dorfinger, P., Koch, T., Stampfl, J., Moszner, N., Liska, R., 2016. Rapid formation of regulated methacrylate networks yielding tough materials for lithography-based 3D printing. Polym. Chem. 7 (11), 2009–2014. https://doi.org/10.1039/C5PY02009C.

Gosch, A., Arbeiter, F.J., Berer, M., Pinter, G., 2018. Comparison of J-integral methods for the characterization of tough polypropylene grades close to the glass transition temperature. Eng. Fract. Mech. 203, 2–17. https://doi.org/10.1016/j.engfracmech.2018.06.002.

Grellmann, W., Langer, B., 2017. Deformation and fracture behaviour of polymer materials. Springer Series in Materials Science 247. Springer International Publishing, Cham, pp. s.l.

Gu, G.X., Takaffoli, M., Buehler, M.J., 2017. Hierarchically enhanced impact resistance of bioinspired composites. Adv. Mater. 29 (28). https://doi.org/10.1002/adma.201700060.

Gurtin, M.E., 2000. Configurational Forces as Basic Concepts of Continuum Physics 137 Springer New York, New York, NY.

Hale, G.E., Ramsteiner, F., 2001. J-Fracture toughness of polymers at slow speed. Pages 123–157 in: Fracture Mechanics Testing Methods For Polymers, Adhesives and Composites. Elsevier.

Huajian, G., 1991. Fracture analysis of nonhomogeneous materials via a moduli-perturbation approach. Int. J. Solids Struct. (International Journal of Solids and Structures) 27 (13), 1663–1682. https://doi.org/10.1016/0020-7683(91)90068-Q.

Jia, Z., Wang, L., 2019. 3D printing of biomimetic composites with improved fracture toughness. Acta. Mat. 173, 61–73. https://doi.org/10.1016/j.actamat.2019.04.052.

Jia, Z., Yu, Y., Hou, S., Wang, L., 2019. Biomimetic architected materials with improved dynamic performance. J. Mech. Phys. Solids 125, 178–197. https://doi.org/10.1016/j.jmps.2018.12.015.

Karalekas, D., Aggelopoulos, A., 2003. Study of shrinkage strains in a stereolithography cured acrylic photopolymer resin. J. Mater. Process. Technol. (Journal of Materials Processing Technology) 136 (1–3), 146–150. https://doi.org/10.1016/S0924-0136(03)00028-1.

Karger-Kocsis, J., Varga, J., Ehrenstein, G.W., 1997. Comparison of the fracture and failure behavior of injection-molded α- and β-polypropylene in high-speed three-point bending tests. J. Appl. Polym. Sci. 64 (11), 2057–2066. https://doi.org/10.1002/(SICI)1097-4628(19970613)64:11<2057:AID-APP1>3.0.CO;2-I.

Kolednik, O., 2000. The yield stress gradient effect in inhomogeneous materials. Int. J. Solids Struct. (International Journal of Solids and Structures) 37 (5), 781–808. https://doi.org/10.1016/S0020-7683(99)00060-8.

Kolednik, O., Kasberger, R., Sistaninia, M., Predan, J., Kegl, M., 2019. Development of damage-tolerant and fracture-resistant materials by utilizing the material inhomogeneity effect. J. Appl. Mech. 86, 1–12.

Kolednik, O., Predan, J., Fischer, F.D., 2010. Cracks in inhomogeneous materials: comprehensive assessment using the configurational forces concept. Eng. Fract. Mech. 77 (14), 2698–2711. https://doi.org/10.1016/j.engfracmech.2010.07.002.

Kolednik, O., Predan, J., Fischer, F.D., Fratzl, P., 2011. Bioinspired design criteria for damage-resistant materials with periodically varying microstructure. Adv. Funct. Mater. 21 (19), 3634–3641. https://doi.org/10.1002/adfm.201100443.

Lach, R., Grellmann, W., 2017. Time-Dependent fracture behaviour of polymers at impact and quasi-static loading conditions. In: Grellmann, W., Langer, B. (Eds.), Pages 3–21 in: Deformation and Fracture Behaviour of Polymer Materials. Springer International Publishing, Cham, pp. s.l.

Lach, R., Krolopp, T., Hutar, P., Grellmann, W., 2014. Influence of the interface and the additional layer on the stable crack propagation through polyolefin bilayered structures. Procedia Mater. Sci. 3, 867–872. https://doi.org/10.1016/j.mspro.2014.06.141.

Lach, R., Krolopp, T., Hutař, P., Nezbedova, E., Grellmann, W., 2016. Short-Term stable crack propagation through polyolefin Single- and Bilayered structures - Influence of welding. Composition and Direction of Crack Propagation. SSP 258, 538–541. https://doi.org/10.4028/www.scientific.net/SSP.258.538.

Lach, R., Krolopp, T., Hutař, P., Nezbedová, E., Grellmann, W., 2017. Influence of welding and composition on the short-term stable crack propagation through polyolefin Single- and Bilayered structures. In: Grellmann, W., Langer, B. (Eds.), Pages 211–227 in: Deformation and Fracture Behaviour of Polymer Materials. Springer International Publishing, Cham, pp. s.l.

Lach, R., Seidler, S., Grellmann, W., 2005. Resistance against the intrinsic rate of fracture mechanics parameters for polymeric materials under moderate impact loading. Mech. Time-Depend. Mater. 9 (2–3), 103–119. https://doi.org/10.1007/s11043-005-1084-y.

Levi, C., Barton, J.L., Guillemet, C., Le Bras, E., Lehuede, P., 1989. A remarkably strong natural glassy rod: the anchoring spicule of the monorhaphis sponge. J. Mater. Sci. Lett. 8 (3), 337–339. https://doi.org/10.1007/BF00725516.

Ligon-Auer, S.C., Schwentenwein, M., Gorsche, C., Stampfl, J., Liska, R., 2016. Toughening of photo-curable polymer networks: a review. Polym. Chem. 7 (2), 257–286. https://doi.org/10.1039/C5PY01631B.

Mao, L.-.B., Gao, H.-.L., Yao, H.-.B., Liu, L., Cölfen, H., Liu, G., Chen, S.-.M., Li, S.-.K., Yan, Y.-.X., Liu, Y.-.Y., Yu, S.-.H., 2016. Synthetic nacre by predesigned matrix-directed mineralization. Science 354 (6308), 107–110. https://doi.org/10.1126/science.aaf8991.

Martínez, A.B., León, N., Arencón, D., Rodríguez, J., Salazar, A., 2013. On the effect of the different notching techniques on the fracture toughness of petg. Polym. Test. 32 (7), 1244–1252. https://doi.org/10.1016/j.polymertesting.2013.07.016.

Martínez, A.B., Salazar, A., León, N., Illescas, S., Rodríguez, J., 2016. Influence of the notch-sharpening technique on styrene-acrylonitrile fracture behavior. J. Appl. Polym. Sci. 133 (32), 11. https://doi.org/10.1002/app.43775.

Maugin, G.A., 1995. Material forces: concepts and applications. Appl. Mech. Rev. 48 (5), 213. https://doi.org/10.1115/1.3005101.

Meijer, H.E.H., Govaert, L.E., 2005. Mechanical performance of polymer systems: the relation between structure and properties. Prog. Polym. Sci. 30 (8–9), 915–938. https://doi.org/10.1016/j.progpolymsci.2005.06.009.

Miserez, A., Weaver, J.C., Thurner, P.J., Aizenberg, J., Dauphin, Y., Fratzl, P., Morse, D.E., Zok, F.W., 2008. Effects of laminate architecture on fracture resistance of sponge biosilica: lessons from nature. Adv. Funct. Mater. 18 (8), 1241–1248. https://doi.org/10.1002/adfm.200701135.

Morgan, E.F., Barnes, G.L., Einhorn, T.A., 2013. The bone organ system. Pages 3–20 in: Osteoporosis. Elsevier.

Mostegel, F.H., Roth, M., Gassner, M., Oesterreicher, A., Piock, R., Edler, M., Griesser, T., 2016. Vinylcarbonates as low-toxic monomers for digital ink-jet inks: promising alternatives to acrylate based systems. Prog. Org. Coat. 94, 116–123. https://doi.org/10.1016/j.porgcoat.2016.01.003.

Muju, S., 2000. Crack propogation in bimaterial multilayered periodically microcracking composite media. Compos. Sci. Technol. 60 (12–13), 2213–2221. https://doi.org/10.1016/S0266-3538(00)00016-6.

Müller, W.E.G., Wang, X., Cui, F.-.Z., Jochum, K.P., Tremel, W., Bill, J., Schröder, H.C., Natalio, F., Schlossmacher, U., Wiens, M., 2009. Sponge spicules as blueprints for the biofabrication of inorganic-organic composites and biomaterials. Appl. microbiol. biot. 83 (3), 397–413. https://doi.org/10.1007/s00253-009-2014-8.

Müller, W.E.G., Wang, X., Kropf, K., Ushijima, H., Geurtsen, W., Eckert, C., Tahir, M.N., Tremel, W., Boreiko, A., Schlossmacher, U., Li, J., Schröder, H.C., 2008. Bioorganic/inorganic hybrid composition of sponge spicules: matrix of the giant spicules and of the comitalia of the deep sea hexactinellid monorhaphis. J. Struct. Biol. 161 (2), 188–203. https://doi.org/10.1016/j.jsb.2007.10.009.

Murali, P., Bhandakkar, T.K., Cheah, W.L., Jhon, M.H., Gao, H., Ahluwalia, R., 2011. Role of modulus mismatch on crack propagation and toughness enhancement in bioinspired composites. Phys. Rev. E 84 (1), 739. https://doi.org/10.1103/PhysRevE.84.015102.

Náhlík, L., Šestáková, L., Hutař, P., Knésl, Z., 2010. Generalized linear elastic fracture mechanics: an application to a crack touching the bimaterial interface. KEM 452–453, 445–448. https://doi.org/10.4028/www.scientific.net/KEM.452-453.445.

Nylander-French, L.A., French, J.E., 1998. Tripropylene glycol diacrylate but not ethyl acrylate induces skin tumors in a twenty-week short-term tumorigenesis study in tg.ac (v-Ha-ras) mice. Toxicol. Pathol. (Toxicologic pathology) 26 (4), 476–483. https://doi.org/10.1177/019262339802600403.

Oesterreicher, A., Ayalur-Karunakaran, S., Moser, A., Mostegel, F.H., Edler, M., Kaschnitz, P., Pinter, G., Trimmel, G., Schlögl, S., Griesser, T., 2016a. Exploring thiol-yne based monomers as low cytotoxic building blocks for radical photopolymerization. J. Polym. Sci. Part A: Polym. Chem. 54 (21), 3484–3494. https://doi.org/10.1002/pola.28239.

Oesterreicher, A., Gorsche, C., Ayalur-Karunakaran, S., Moser, A., Edler, M., Pinter, G., Schlögl, S., Liska, R., Griesser, T., 2016b. Exploring network formation of tough and biocompatible thiol-yne based photopolymers. Macromol. rapid comm. 37 (20), 1701–1706. https://doi.org/10.1002/marc.201600369.

Oesterreicher, A., Moser, A., Edler, M., Griesser, H., Schlögl, S., Pichelmayer, M., Griesser, T., 2017. Investigating photocurable thiol-yne resins for biomedical materials. Macromol. Mater. Eng. 302 (5), 1600450. https://doi.org/10.1002/mame.201600450.

Oesterreicher, A., Wiener, J., Roth, M., Moser, A., Gmeiner, R., Edler, M., Pinter, G., Griesser, T., 2016c. Tough and degradable photopolymers derived from alkyne monomers for 3D printing of biomedical materials. Polym. Chem. 7 (32), 5169–5180. https://doi.org/10.1039/c6py01132b.

Rice, J.R., 1968. A path independent integral and the approximate analysis of strain concentration by notches and cracks. J. Appl. Mech. 35 (2), 379. https://doi.org/10.1115/1.3601206.

Ritchie, R.O., 2011. The conflicts between strength and toughness. Nat. Mater. 10 (11), 817–822. https://doi.org/10.1038/nmat3115.

Salazar, A., Frontini, P.M., Rodríguez, J., 2014. Determination of fracture toughness of propylene polymers at different operating temperatures. Eng. Fract. Mech. 126, 87–107. https://doi.org/10.1016/j.engfracmech.2014.04.023.

Salazar, A., Rico, A., Rodríguez, S., Navarro, J.M., Rodríguez, J., 2012. Relating fracture behavior to spherulite size in conrolled-rheology polypropylenes. Polym. Eng. Sci. 52 (4), 805–813. https://doi.org/10.1002/pen.22145.

Salazar, A., Rodríguez, J., Arbeiter, F., Pinter, G., Martínez, A.B., 2015. Fracture toughness of high density polyethylene: fatigue pre-cracking versus femtolaser, razor sharpening and broaching. Eng. Fract. Mech. 149, 199–213. https://doi.org/10.1016/j.engfracmech.2015.07.016.

Schwalbe, K.-.H., Neale, B., 1995. A procedure for determining the fracture behaviour of materials-The unified fracture mechanics test method efam gtp 94. Fat. Fract. Eng. Mater. Struct. (Fatigue & Fracture of Engineering Materials and Structures) 18 (4), 413–424. https://doi.org/10.1111/j.1460-2695.1995.tb01185.x.

Seidler, S., Koch, T., Grellmann, W., 2001. Crack tip deformation and toughness in polypropylenes. In: 10th International Conference on Fracture (ICF 10), pp. 120–125.

Simha, N.K., Fischer, F.D., Kolednik, O., Predan, J., Shan, G.X., 2005. Crack tip shielding or anti-shielding due to smooth and discontinuous material inhomogeneities. Int. J. Fract. 135 (1–4), 73–93. https://doi.org/10.1007/s10704-005-3944-5.

Simha, N.K., Fischer, F.D., Kolednik, O., Chen, C.R., 2003. Inhomogeneity effects on the crack driving force in elastic and elastic–plastic materials. J. Mech. Phys. Solids 51 (1), 209–240. https://doi.org/10.1016/S0022-5096(02)00025-X.

Sistaninia, M., Kolednik, O., 2014. Effect of a single soft interlayer on the crack driving force. Eng. Fract. Mech. 130, 21–41. https://doi.org/10.1016/j.engfracmech.2014.02.026.

Song, J., Fan, C., Ma, H., Liang, L., Wei, Y., 2018. Crack deflection occurs by constrained microcracking in nacre. Acta. Mech. Sin. 34 (1), 143–150. https://doi.org/10.1007/s10409-017-0724-1.

Woesz, A., Weaver, J.C., Kazanci, M., Dauphin, Y., Aizenberg, J., Morse, D.E., Fratzl, P., 2006. Micromechanical properties of biological silica in skeletons of deep-sea sponges. J. Mater. Res. 21 (08), 2068–2078. https://doi.org/10.1557/jmr.2006.0251.

Wu, K., Zheng, Z., Zhang, S., He, L., Yao, H., Gong, X., Ni, Y., 2019. Interfacial strength-controlled energy dissipation mechanism and optimization in impact-resistant nacreous structure. Mater Des 163, 107532. https://doi.org/10.1016/j.matdes.2018.12.004.

Yadav, R., Goud, R., Dutta, A., Wang, X., Naebe, M., Kandasubramanian, B., 2018. Biomimicking of hierarchal molluscan shell structure via layer by layer 3D printing. Ind. Eng. Chem. Res. 57 (32), 10832–10840. https://doi.org/10.1021/acs.iecr.8b01738.

Yang, Y., Song, X., Li, X., Chen, Z., Zhou, C., Zhou, Q., Chen, Y., 2018. Recent progress in biomimetic additive manufacturing technology: from materials to functional structures. Adv. Mater., e1706539. https://doi.org/10.1002/adma.201706539.

Zak, A.R., Williams, M.L., 1963. Crack point stress singularities at a bi-material interface. J. Appl. Mech. 30 (1), 142. https://doi.org/10.1115/1.3630064.

Zechner, J., Kolednik, O., 2013. Fracture resistance of aluminum multilayer composites. Eng. Fract. Mech. 110, 489–500. https://doi.org/10.1016/j.engfracmech.2012.11.007.

Zhao, H., Yang, Z., Guo, L., 2018. Nacre-inspired composites with different macroscopic dimensions: strategies for improved mechanical performance and applications. NPG Asia Mater 10 (4), 1–22. https://doi.org/10.1038/s41427-018-0009-6.